Int. J. Electrochem. Sci., 17 **(2022)** Article Number: 22083, doi: 10.20964/2022.08.37

International Journal of
ELECTROCHEMICAL
SCIENCE
www.electrochemsci.org

Influences of Chloride on Microstructure and Corrosion Behaviour of Al-Mg-Si alloys in neutral solution

Chenyang Xiao[1], *Yaya Zheng*[1,2,*], *Zhenfeng Xu*[1], *Li Wang*[1]

[1] Department of Materials Engineering, Hunan University of Humanities, Science and Technology, Loudi 417000, China;
[2] Key Laboratory of Safety Design and Reliability Technology for Engineering Vehicle, Changsha University of Science and Technology, Changsha 410114, China)
[*]E-mail: yayazhengcsu@163.com

Received: 2 October 2021 / *Accepted:* 19 November 2021 / *Published:* 4 July 2022

The influences of Cl^- concentration on the corrosion behaviour of Al-Mg-Si alloy were studied by using scanning electron microscopy (SEM), transmission electron microscopy (TEM) and electrochemical analysis. The results show that the microstructures primarily consist of precipitate free zone (PFZ), large-size MgSi-riched dispersed phase and β′ precipitates. The corrosion type and corrosion behaviour of Al-Mg-Si are greatly affecting by Cl^- concentration. With the increase in Cl^- concentration, the open circuit potential (OCP) and corrosion resistance of the alloy decrease. In 1.0 wt. % NaCl solution, slight pitting corrosion occurs around MgSi phase. In 3.5 wt. % NaCl solution, obvious intergranular corrosion (IGC) and hemispherical pitting corrosion appear. In 5.5 wt. % NaCl solution, corrosion kinetic of the Al-Mg-Si alloy are significantly enhanced, making it susceptible to severe overall corrosion. High concentration of Cl^- leads to rapid dissolution of the passivation film and serious corrosion.

Keywords: Al-Mg-Si alloy; corrosion behaviour; Cl^- concentration; passivation film; microstructure

1. INTRODUCTION

The corrosion of metal materials is largely attributed to the spontaneous process of phase change due to chemical or electrochemical action, leading to material failure. Al-Mg-Si alloy, as a heat-treatable and strengthened alloy, has high strength and corrosion resistance, has been used in various fields of the national economy and national defense construction. Such as manufacturing aircraft cabins, fuselage skins and wings, ship hulls and their superstructures, etc. But they are susceptible to different kinds of corrosion in the service process, such as pitting corrosion, intergranular corrosion (IGC) and exfoliation corrosion in the corrosive solution containing Cl^- ions. The appearances of these corrosion phenomenons greatly reduce the service life of aluminum alloy components and cause significant direct or indirect

economic losses [1-3]. Al-Mg-Si alloy is an amphoteric metal resistant to acid and alkali solution in some extent. In neutral or weak acid solutions, the Al-Mg-Si alloys have high stability due to the existence of continuous and dense oxide passivation film on the surface. However, in the service process, chemical corrosion, electrochemical corrosion and stress corrosion inevitably occur due to the environment or the microstructural characteristics of the material itself [4-5]. Finally, the original strength is lost, leading to the failure of components [6-8]. It is significant to study the corrosion behaviours and analyze their corrosion mechanism for improving the service life, improving economic benefits and protecting the natural environment.

Al-Mg-Si alloys are prone to corrosion in some salt solutions. Among them, halogen ions such as chloride ions play a "unique" role in promoting the dissolution of alloy passivation oxide film. The behaviour of alloys in Cl^- containing solution has been studied extensively. The second phase plays an important role in the local corrosion. For Al-Mg-Si alloys, some researchers believe that IGC sensitivity is the result of micro-current coupling between AlCu, AlCuMg, or MgSi precipitates and adjacent precipitate free zones (PFZ) [9-11]. Luo et al. [12] studied the corrosion process of Al-Mg-Si alloy in a solution containing Cl^-. The results showed that the IGC sensitivity of the alloy was strongly related to the Cu content, Mg/Si ratio and heat treatment. The precipitates and PFZ at the grain boundary were the main initiation points of anodic corrosion.

The corrosion of Al-Mg-Si alloy corrosion is affected not only by the alloy structure and composition, but also by the surrounding environment, such as humidity, salinity, pH value and so on. Tan et al. [15] studied the effects of NaCl concentration solutions on the electrochemical behaviour of Al-Mg-Si alloy. The results show that the increase in Cl^- concentration greatly promotes the occurrence of pitting corrosion. Li et al. [16-17] found that the corrosion of Al-Mg-Si alloy originated from the MgSi phase around the grain boundary in 0.6 M NaCl (pH3.5) solution. Chylak et al. [18] studied the corrosion behaviour of Al-Mg-Si alloy in MgCl solution. The results showed that the pitting corrosion and local corrosion were observed in low concentration Cl^- solution. Zhao et al. [19] found that the corrosion behaviour of Al-Mg-Si alloy in different salinity solutions was obviously different.

Furthermore, due to the complexities of the corrosion environments. Corrosion behaviour of Al-Mg-Si alloy in Cl^- containing solution still not well understood. No definite theory has been established to analyse the corrosion behaviour of Al-Mg-Si alloys, and still difficult to unify the corrosion behaviour of the Al-Mg-Si alloys. Therefore, this work studied concentration on the corrosion behaviour and electrochemical behaviour of the Al-Mg-Si alloy in Cl^- containing solution by analysing the microstructures and electrochemical behaviour of the Al-Mg-Si alloy, to clarify the corrosion mechanism of Al-Mg-Si alloy in different Cl^- concentration solutions.

2. MATERIALS AND METHODS

The aluminum alloy used in the experiment was melted by graphite crucible in well resistance furnace. The alloy composition is shown in Table 1. Firstly, the alloy ingot was homogenized annealing at 520 ℃ / 24 h, followed immediately hot rolled to obtain 8mm plate (80% deformation). Subsequently, the plate was subjected to solution treatment for 520 ℃ × 2 h followed immediately quenched into cold

water at room temperature, and then subject to 180 ℃ × 6 h peak aging treatment. The peak aged alloy samples were selected for IGC tests. The corrosion solution were NaCl solution with different concentrations (1.0 wt.%, 3.5 wt.%, 5.5 wt.%,). The corrosion temperature is 35 ℃ and the corrosion time is 24 h. The corrosion surface of each sample was polished and cleaned before the immersion. In order to avoid the tested sample long-term exposure to the atmosphere, the sample must be tested immediately after cleaning.

Table 1. Chemical compositions of the studied Al-Mg-Si alloy

Chemical compositions	Mg	Si	Cr	Mn	Zr	Ti
wt.%	2.05	2.29	0.16	0.31	0.15	0.1

The OCP and electrochemical impedance spectroscopy (EIS) are measured by the electrochemical workstation of multi-autolab-m204. The measured area is 10 mm × 10 mm. The test temperature is about 25 ℃, and the frequency range is 10^{-2} Hz ~ 10^{5} Hz. The impedance data were fitted by Zsimpwin software. XJG-OS optical microscope and Sirion-200 scanning electron microscope (SEM) equipped with Genesis-60S energy spectrometer were used to observe the microstructure and corrosion morphology of the alloy samples.

The alloy microstructure was observed on the Tcnai G2 F20 transmission electron microscope. The transmission sample is prepared by double-jet thinning. The test sample is firstly ground and thinned to 70 μm on the grinding machine, and then prepare a thin disc with a diameter of 3 mm on the punching machine. Constant voltage double injection mode is adopted. The double spray solution to electrolysis is 30% HNO_3 + 70% CH_3OH. The temperature of double-jet is - 25℃. The voltage is 25V.

3. RESULTS AND DISCUSSION

3.1 Microstructures

Fig. 1 shows the SEM image of the sample and the corresponding element distribution results. The energy dispersive X-ray spectroscopy (EDS) results show that there are two kinds of large size phases in the grain boundary. The white contrast phases are FeMn crystallization phases rich in Mn and Fe elements. The, and the gray-black contrast phases are the MgSi phase. These two kinds of coarse phases are formed during the casting process. The FeMn phase has a high crystallization temperature and extremely low solubility in the aluminum matrix, resulting in the inability to re-dissolve in the following solution heat-treatment process [11]. The MgSi phase cannot be entirely dissolved and remains distributed at the grain boundaries.

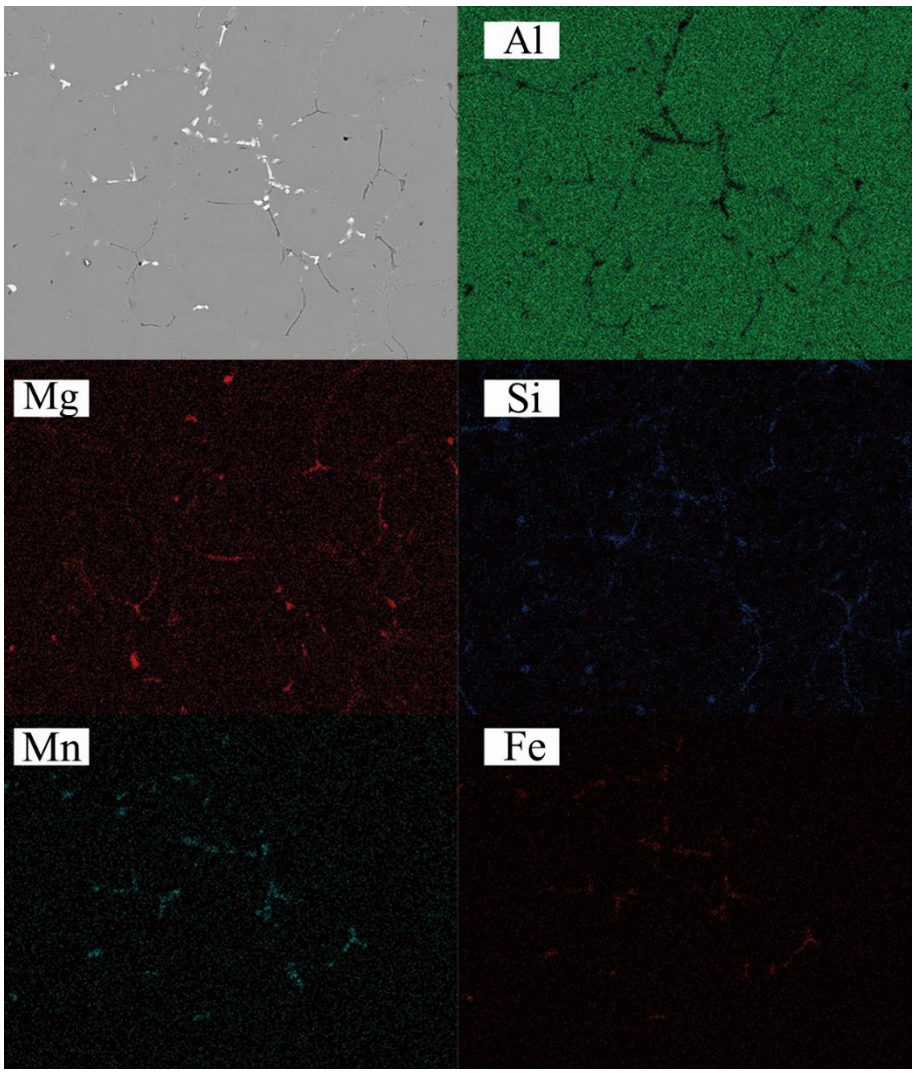

Figure 1. SEM image and EDS element mappings of the Al-Mg-Si alloy with T6 heat-treatment

In addition to the above coarse phase, there are many fine metastable precipitates and a large dispersed phase. Fig. 2 shows the TEM microstructures and accompanying EDS results of the grain boundary precipitates. It can be seen that the alloy exhibits two characteristic phases and PFZ with a width of about 32 nm in the grain boundary. One is short rod-shaped precipitate with intermittent distribution, and a diameter of more than 50 nm. According to the relevant literatures, it can be concluded that the short rod-shaped phase is β′ phase (Fig.2c). According to the corresponding EDS results (Fig. 2b), another one is spherical-like FeMnSi dispersed precipitates. During the ageing heat-treatment process, these dispersed phases can act as the nucleation site of the metastable phase, and improve the mechanical properties [12].

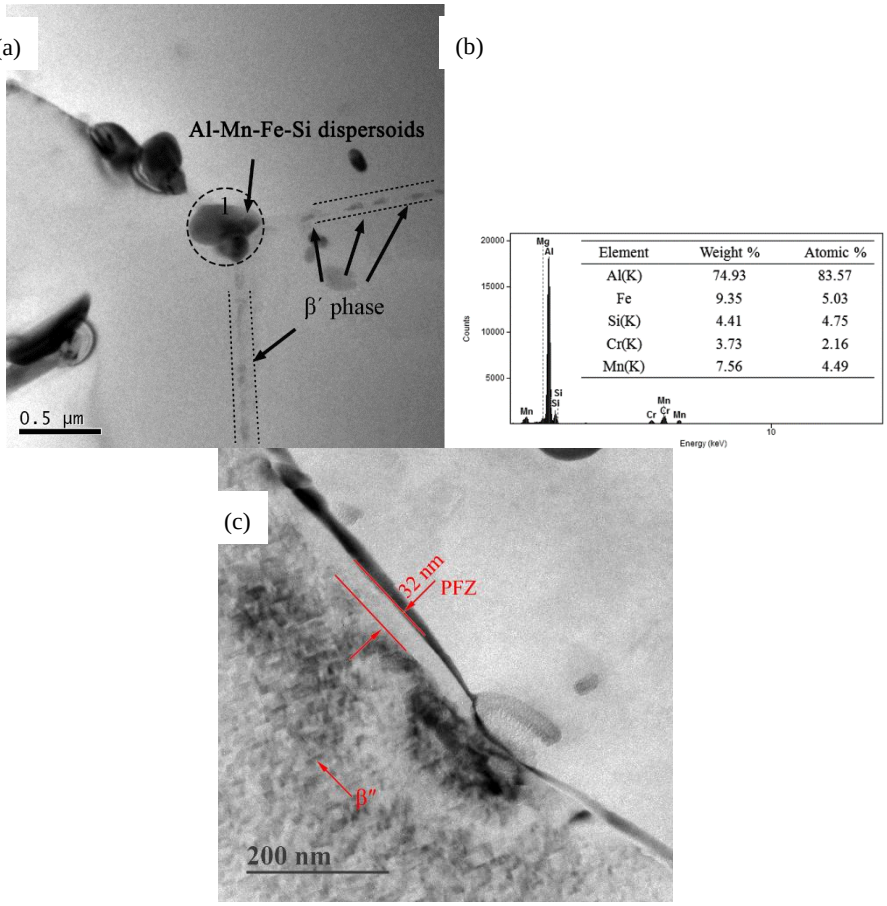

Figure 2. TEM images of the grain boundary precipitates of the alloy and corresponding EDS results (a) TEM images of the alloy; (b) corresponding EDS results of particle 1 marked in (a); (c) TEM image for showing the existence of PFZ.

The typical FeMnSi dispersed phase in the T6 Al-Mg-Si alloy structure was further characterized by high-angle circular dark-field scanning transmission microscope (HAADF-STEM), as shown in Fig.3. There is a certain width of PFZ around the FeMnSi phase, as shown in Fig.3(b). The composition of the phase is Mg, Si, Mn, and Cr and other alloying elements. These dispersed phases are formed during high-temperature heat treatment, such as the homogenization cooling process and quenching process. They absorb surrounding Mg, Si, and other solute atoms and grow up during the subsequent ageing heat-treatment, forming a certain width of PFZ. The significant composition difference between the α(Al) matrix and these phases, leading to large potential differences between them. Studies have shown that in a neutral solution containing 3.5 wt.% NaCl, the self-corrosion potentials for α(Al) and Mg_2Si phases are -0.876 V and -1.160 V, respectively [16]. The potentials for FeMnSi phase are higher than Al matrix. This potential difference inevitably leads to electrochemical corrosion of the alloy.

3.2 Corrosion behaviour

Fig. 3 shows the SEM images of the corroded sample in NaCl solutions for 24 h and corresponding EDS results. It can be seen that when the NaCl concentration is 1.0 wt.%, the sample

shows some annular corrosion pits around the MgSi phase. When the NaCl concentration is 3.5 wt.%, the alloy exhibits pitting corrosion and a slight IGC network (Fig.3(c,d)). Part of the second phase is basically dissolved in the corrosion pits. From the above results, there are many kinds of structures mainly including FeMn phase, MgSi phase and PFZ on the surface. The uniformity of microstructure and distribution of composition inevitably leads to the existence of defects on the alloy oxide film. In a corrosive solution containing Cl^-, corrosion Initiation starts from these places. The FeMnSi phase acts as a cathode during this corrosion process and leads to corrosion of the surrounding anode structures, including aluminum matrix, PFZ and MgSi. When the concentration of NaCl is 5.5 wt.%, the corrosion morphology of the sample varies greatly, showings overall corrosion. EDS result of position 2 in Fig.3(f) shows that the alloy corrosion layer is mainly composed of O, Al and Mg, with a very high proportion of O. Cl^- can be adsorbed on the alloy surface and enter into the surface passivation film by the force of electric field [20,21]. Compared with the original film, the ion transport rate of the passivation film infiltrated with Cl^- is faster, which accelerates the dissolution of Al matrix and releases metal ions, as well as the diffusion of released metal ions into the solution through the metal oxide layer [22]. Therefore, the high concentration of Cl^- can aggravate the dissolution of the oxide film and promote the overall corrosion of the alloy.

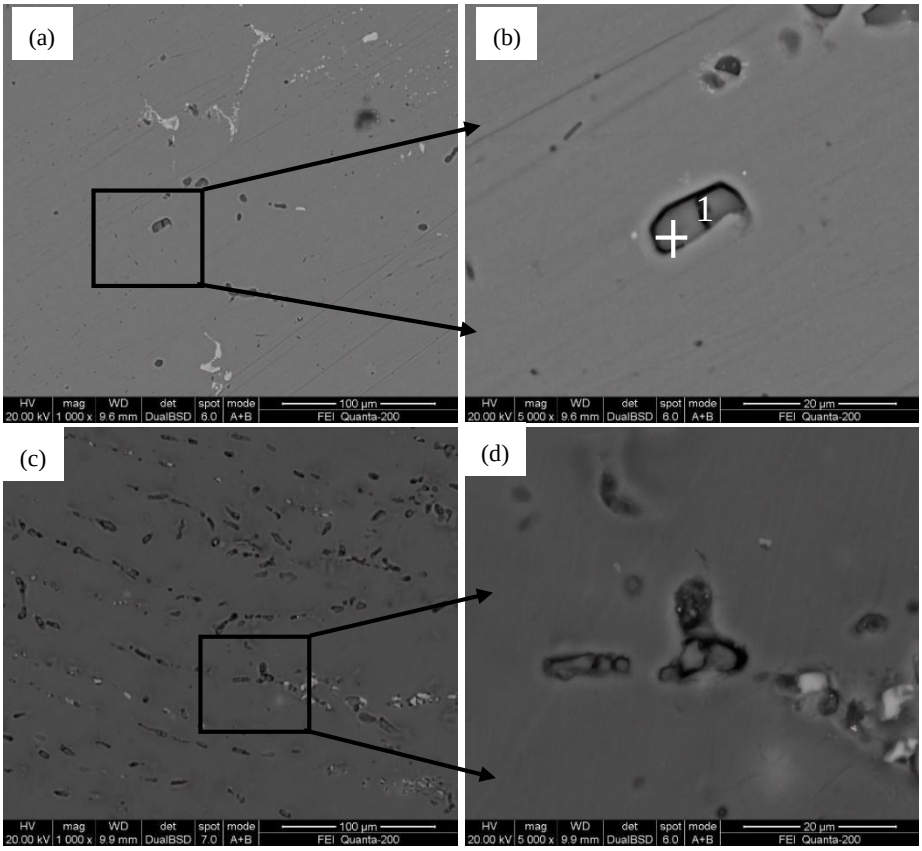

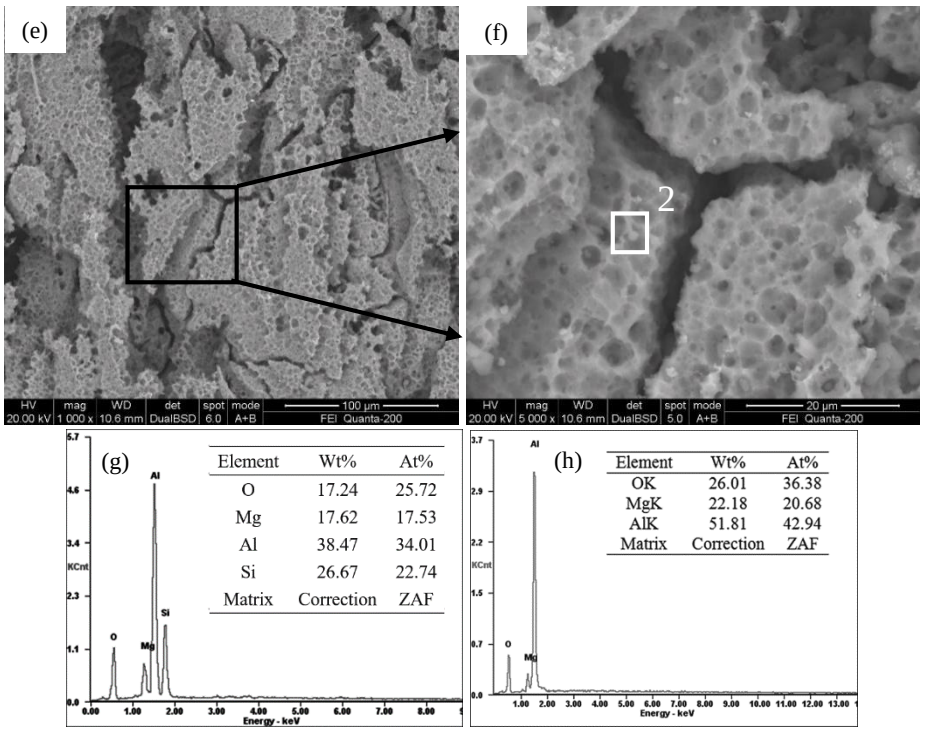

Figure 3. SEM images of the Al-Mg-Si alloy after corrosion in NaCl solution with different concentration and corresponding EDS analysis (a, b) 1.0 wt.%; (c, d) 3.5 wt.%; (e, f) 5.5 wt.%; (g, h) corresponding EDS results of particles 1 and 2 marked in Fig.3(d) and Fig.3(f), respectively

3.3 OCP

Fig. 4 shows the open circuit potential (OCP) various curves of the T6 samples in NaCl solutions with different concentration. During the first 1500 s of immersion, the OCP show different variation tendencies in different concentrations of NaCl solution. The variation of OCP depends on the initiation and growth process of alloy corrosion, and can reflect the competitive relationship between the protection of alloy passivation film and corrosion during the immersion process [22,23]. At the end of immersion, the relatively stable OCP value indicates that the corrosion and passivation reach a relatively stable state. In 1.0 wt.% NaCl solution, the OCP value increases with the increase of immersion time, and remains relatively stable after immersion 4500 s, maintaining at -0.81 V. When the concentration of NaCl is 3.5 wt.%, the OCP increases rapidly within the first 1500 s of immersion. Then, it is stabilized at -0.86 V. When the concentration of NaCl increases to 5.5 wt.%, the OCP value rises sharply at the beginning of immersion, then decreases slowly after 1000 s, and finally remains relatively stable at -0.96 V.

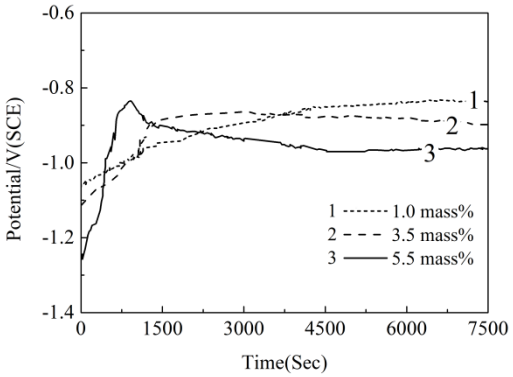

Figure 4. Plots of open circuit potential vs. time of the Al-Mg-Si alloy in NaCl solution with different concentrations

The oxide film of Al-Mg-Si alloy has certain corrosion resistance in the corrosion solution containing Cl^-. Therefore, at a lower concentration of NaCl solution, due to the relatively stable anticorrosion effects of the surface passivation film, the time for reaching a stable corrosion state is longer, exceeding 4500 s. As the concentration of Cl^- increases, the protective ability of the passivation film infiltrated Cl^- is reduced, and shortens the time to reach the equilibrium state between corrosion and protection of the passivation film. When the NaCl concentration is 5.5 wt.%, the high concentration of Cl^- accelerates the dissolution process. The dissolution of passivation film infiltrated with Cl^- intensify, the OCP value gradually decreases.

3.4 EIS

The EIS tests can explain the electrochemical performance and corrosion behaviour of Al-Mg-Si alloy more clearly. As shown in Fig.5, the high frequency parts of the EIS spectrums of the Al-Mg-Si alloy in different concentrations of NaCl solution exhibit capacitive reactance arc. For low frequency parts, as the Cl^- concentration increases, the capacitive reactance arc transforms into inductive reactance arc. Some scholars believe that the low frequency part is related to the local dissolution of the passivation film [24,25]. When there is no condition causing pitting corrosion, the thickness of the passivation film remains stable. When Cl^- is present, the dissolved passivation layer results in the inductive arc appear in the low frequency part. With the increase in Cl^- concentration, the inductive arc gradually shrinks. For the high-frequency part, the size of the capacitive reactance arc is related to the adsorption of Cl^- or corrosion products on the surface of the passivation film, the adsorption phenomenon leads to the appearance of double-layer capacitors in equivalent corrosion circuit [26].

In a lower concentration of NaCl solution, the protective passivation film can effectively inhibit the dissolution of the alloy matrix. As the concentration of the NaCl solution increases, the concentration of Cl^- adsorbed on the passivation film increases, penetrating into the passivation film, and weakening the protection of the passivation film [27]. Which increases the active area of the alloy, leading to local rapid dissolution of the Al-Mg-Si alloy. Therefore, with the increase of Cl^- concentration in the corrosion solution, the low-frequency part of the alloy shifts from capacitive reactance arc to inductive reactance arc, and its radian is related to the thickness of the remaining passivation film.

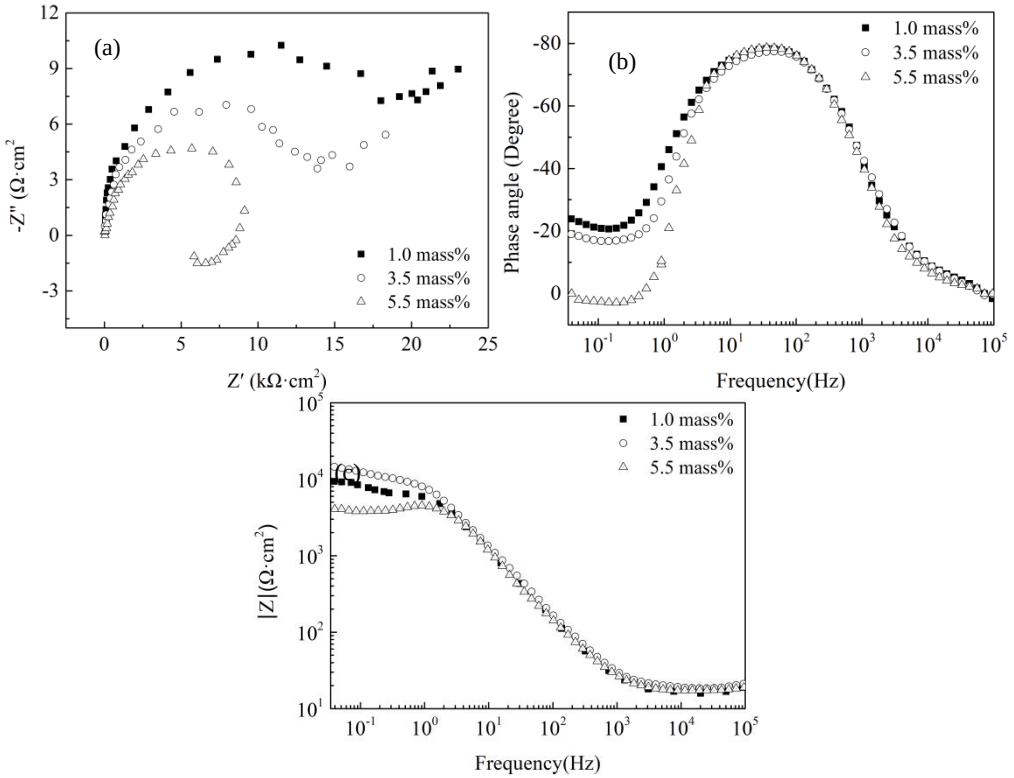

Figure 5. EIS Nyquist and Bode plots of the Al-Mg-Si alloy in NaCl solution with various concentration (a) Nyquist curves; (b, c) Bode plots

According to the EIS results of Al-Mg-Si alloy, two equivalent circuits are proposed to fit the EIS results (Fig.6). Fig.6(a) is the EIS fitting result of the alloy in 1.0 wt.% and 3.5 wt.% NaCl solution. Fig.6(b) corresponds to the EIS fitting result of the alloy in 5.5 wt.% NaCl solution. The relevant electrochemical parameters are shown in Table 2. R_s, R_{surf}, and R_{ct} are solution resistance, surface oxide film resistance, and charge transfer resistance, respectively. Q_1 and Q_2 are the constant phase angle elements of the surface oxide film and electric double-layer capacitance, respectively. L is an inductive element related to the relaxation process. The appearance of relaxation phenomenon is generally related to the concentrated adsorption of Cl^- in the local area of the alloy surface, such as the active area around the second phase [28].

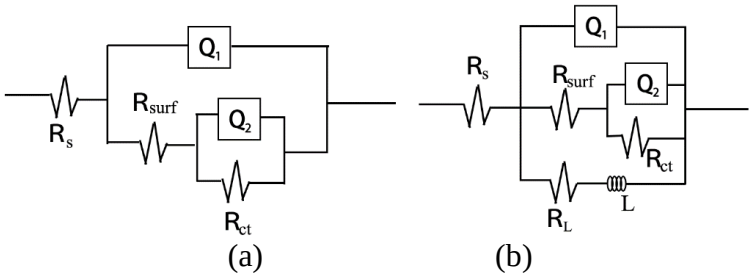

Figure 6. Equivalent circuit models used for curve fitting of EIS results (a) 1.0 wt.% NaCl and 3.5 wt.% NaCl; (b) 5.5 wt.% NaCl.

Table 2. EIS fitting results of the Al-Mg-Si alloy in NaCl solution with different concentration

NaCl concentration (wt.%)	R_s/(Ω·cm^{-2})	R_{surf} /(Ω·cm^{-2})	R_{ct} /(Ω·cm^{-2})	L/(H·cm^{-2})	R_L/(Ω·cm^{-2})	Q_1/(μF·cm^{-2})	n_1	Q_2/(μF·cm^{-2})	n_2
1.0	88.43	11452	9537	-	-	12	0.94	116	0.94
3.5	26.94	11992	3247	-	-	14	0.94	178	0.96
5.5	13.45	1071	4357	775	4572	10		256	0.97

With the increase in NaCl concentration, the total resistance (R_{surf} + R_{CT}) of the Al-Mg-Si alloy decreases gradually. In 1.0 wt.% and 3.5 wt.% NaCl solution, the total resistance is greater than 15 KΩ•cm^{-2}. When the concentration of NaCl is 5.5 wt.%, the total resistance is less than 6 KΩ•cm^{-2}. With the increase of Cl^- concentration, the sum of R_{surf} and R_{CT} decreased gradually. This may be attributed to a combined effects from the dissolution and regeneration of the surface film. In low concentration NaCl solution, the newborn oxide film can quickly cover the corrosion sites, and inhibit further corrosion. When the NaCl concentration is 5.5 wt.%, the high concentration Cl^- adsorbed in the alloy surface, resulting in overall corrosion, so that the aluminum matrix is completely exposed to the corrosive solution. Therefore, the corrosion resistance decreases sharply.

Because of the inhomogeneous chemical and physical properties of the passivation film, defects in multicomponent Al-Mg-Si alloys are unavoidable. Corrosion derived from the passivation film's weakness sites, such as the surrounding area of MgSi phase, FeMnSi phase, and' phase, especially at the grain boundary.. With the progress of corrosion, MgSi phase preferentially corrodes Mg and transforms into Si-rich phase. FeMnSi phase and these Si-rich phases act as cathodes in the following corrosion process. PFZ greatly promotes the electrochemical corrosion along grain boundaries by anodic dissolution of PFZ. Cl^- infiltrates into the corrosion tip along anodic dissolution ditch and combines with H^+ to form a local strong acid environment [14]. Which promotes the development of corrosion into the interior of the alloy, causing severe corrosion. The passivation film dissolves completely when the Cl- concentration reaches a certain level. As a result, the alloy's corrosion resistance drops sharply, leading to overall corrosion.

4. CONCLUSIONS

This paper focused on microstructures and the effects of Cl^- concentration on the Al-Mg-Si alloys corrosion behavior. The following are the main conclusions:

(1)With the increase in Cl^- concentration, OCP and corrosion resistance of the alloy decrease. In 1.0 wt.% NaCl solution, slight pitting corrosion occurs around MgSi phase. In 3.5 wt.% NaCl solution, obvious IGC and hemispherical pitting corrosion appear. The Al-Mg-Si alloy's corrosion kinetics are maximum in a 5.5 wt.% NaCl solution, and it is susceptible to severe overall corrosion.

(2)The initial corrosion site of Al-Mg-Si alloy occurs on the anode phases, such as MgSi and PFZ. The high concentration of Cl^- causes the passivation film to dissolve quickly and the alloy to corrode severely.

(3) The corrosion sensitivity degree of the Al-Mg-Si alloy can be well validated by corrosion resistance. The decrease OCP value and the decrease of total corrosion resistance are related to the dissolution of defects results from the uniformity of microstructure and distribution of composition.

ACKNOWLEDGEMENTS
This study is supported by the Open Fund of Hunan Province Key Laboratory of Safety Design and Reliability Technology for Engineering Vehicle. No. KF1904.

References

1. G.S. Frankel, T. Li and J.R. Scully. *J. Electrochem. Soc*., 164 (2017) 180.
2. H.X. Guo, B.T. Lu and J.L. Luo. *Electrochim. Acta*, 52 (2006) 1108.
3. H. Li, P. Zhao, Z.X. Wang, Q.Z. Mao, B.J. Fang, R.G. Song and Z.Q. Zheng. *Corros. Sci*., 107 (2016) 113.
4. L.T. Yin, Y. Jin, L. Chrlstofer and J.S. Pan. *Electrochim. Acta*, 192 (2016) 310.
5. Y.Y. Zheng, B.H. Luo, Z.H. Bai, J.Wang and Y. Yin. *Metals*, 7 (2017) 387.
6. U. Trdan and J. Grum. *Corros. Sci*., 59 (2012) 324.
7. Y.J. Tan, E.S. Bail and A.B. Kinsell. *Corros. Sci*., 43 (2001) 1905.
8. L.L. Li, B. Zhang, B. Tian, Y. Zhou, J.Q. Wang, E.H. Han and W. Ke. *J. Electrochem. Soc*., 164 (2017) 240.
9. Z. Li, C. Li, Z.M. Gao, Y.C. Liu, X.F. Liu, Q.Y. Guo, L.M. Yu and H.J. Li. *Mater. Charact*., 110 (2015) 170.
10. E. Mccafferty. *Corros. Sci.*, 47 (2005) 3202.
11. S.S. Wang, M.D. Cheng, L.C. Tsao and T.H. Chuang. *Mater. Charact*., 47 (2001) 401.
12. Y.Y. Zheng, B.H. Luo, Z.H. Bai and C. He. *JOM*, 71 (2019) 4737.
13. R.P. Wahi and M.V. Heimendahl. *Mater. Sci. Eng*. A, 24 (1974) 607.
14. M.C. Zhao, M. Liu, G.L. Song and A. Atrens. *Corros. Sci*., 50 (2008) 3168.
15. R.G. Buchheit. *J. Electrochem. Soc*., 142 (1995) 3994.
16. X. Zhan, J.G. Tang, H.Z. Li, X.P. Liang, Y.F. Lu, Y.X. Che, W.B. Tu and Y.D. Zhang. *J. Alloys Compd.,* 819 (2020) 152960.
17. Y. Zou, Q. Liu, Z. Jia, Y. Yuan, L.P. Ding and X.L. Wang. *Appl. Surf. Sci*., 405 (2017) 489.
18. A.B.Y. Lim, W.J. Neo, O. Yauw, B. Chylak, C.L. Gan and Z. Chen, *Microelectron. Reliab*., 56 (2016) 155.
19. Y. Zheng, W.l. Xiao, S.J. Ge, W.T. Zhao, S.J. Hanada, and C.l. Ma, *J. Alloys Compd*., 649 (2015) 291.
20. P. Marcus, V. Maurice and H.H. Strehblow. *Corros. Sci.*, 50 (2008) 2698.
21. D.D. Macdonald. *Electrochim. Acta*, 56 (2011) 1761.
22. Y.T. Zhou, Y.N. Zan, Q.Z. Wang, B.L. Xiao, Z.Y. Ma and X.L. Ma. *Corros.Sci*., 174 (2020) 108808.
23. K.D. Ralston and N. Birbilis. *Corros.*, 66 (2010) 075005.
24. T. Hashimoto, X. Zhou, P. Skeldon and G.E. Thompson. *Electrochim. Acta*, 179 (2015) 394.
25. X.M. Chen, X.N. Wang, Q.P. Dong, J.M. Yu, Z. Zhu and H. Nagaumi. *J. Mater.Res.Technol*., 14 (2021) 1203.
26. Q.J. Zheng, J. Wu, H.H. Jiang, L.L. Zhang, J.Z. Zhao and J. He. *Corros. Sci.*, 179 (2021) 109113.
27. X.X. Zhang, Y. Lv, T. Hashimoto, J.O. Nilsson and X.R. Zhou. *J. Alloys Compd*., 853 (2021) 157228.

28. S. Kumari, S. Wenner, J.C. Walmsley, O. Lunder and K. Nisancioglu. *Corros. Sci*., 158 (2019) 108090.